High-resolution spectroscopy with a molecular beam at 10.6 μm

A. Amy-Klein,* L. F. Constantin, R. J. Butcher,† G. Charton, and Ch. Chardonnet
Laboratoire de Physique des Lasers, CNRS UMR No. 7538, Université Paris 13, 99 avenue J. B. Clément, F-93430 Villetaneuse, France
(Received 18 May 2000; published 1 December 2000)

Molecular spectroscopy in the infrared region is pushed to new limits by using the Ramsey technique of separated fields on a two-photon transition in SF_6 excited using a CO_2 laser. The geometry employed elegantly compensates all Doppler problems, while giving progressively higher resolution for simple optical adjustments. In addition, the molecular beam can be characterized by interrogation of a quasiresonant intermediate level. Fringes are obtained with a periodicity down to 1.5 kHz and a statistical uncertainty of a few $10^{-13}\,\mathrm{Hz}^{-1/2}$. The projection for a frequency standard is in the 10^{-15} range.

DOI: 10.1103/PhysRevA.63.013404 PACS number(s): 42.50.Hz, 33.20.Ea, 42.62.Fi, 06.20.−f

I. INTRODUCTION

CO_2 lasers stabilized on narrow sub-Doppler molecular resonances are widely used as secondary frequency standards in the 9–12-μm spectral region. The saturated fluorescence technique developed by Freed and Javan is commonly used for stabilization onto the CO_2 laser lines because it provides a convenient reference for all laser lines [1]. By use of different CO_2 isotopic species, it provides a dense grid of reference frequencies with accuracies of a few kHz in the infrared region. Alternatively, CO_2 lasers can be locked directly onto saturated absorption lines of molecules. By this means, the CO_2 laser locked onto a saturated absorption resonance of OsO_4 provides a secondary frequency standard in the 10-μm region with very good stability characteristics [2,3]. Its accuracy reaches 10 Hz for the optimal lines [4].

To improve this performance, the well-known strategy is to record narrower and narrower lines; since most of the systematic errors are proportional to the linewidth of the frequency reference, any increase in the experimental resolution will result in an increase in the ultimate accuracy of the frequency standard. A slow molecule detection method [5–7] pushes the transit broadening limit down and the resolution may be improved to a few hundreds of Hz, but with a degraded signal-to-noise ratio (SNR). The alternative possibility of slowing and trapping molecules is very limited for the moment [8].

While molecular spectroscopy using cells is now approaching its limits, the possibility of high-resolution spectroscopy at 10 μm with a molecular beam is less explored. The method of separated fields or Ramsey fringes [9] was extended to the visible domain in the 1970s [10–15] and allows the limit of resolution with a beam to be greatly improved. Several visible frequency standards were developed with this technique. At 10 μm, after the pioneering work of Bordé *et al.* [16], few developments followed [17], although more recently new interest in this technique has emerged [18,19]. Later, some two-photon lines were observed and identified in SF_6 [20,21], opening an opportunity to explore two-photon Ramsey fringes. Thus, molecular-beam spectroscopy seems very promising for a new generation of frequency standards in the infrared.

II. TWO-PHOTON RAMSEY FRINGES

The main point of Ramsey spectroscopy is to provide a signal of which the linewidth is no longer limited by the transit time through the laser beam. For this purpose, the single interaction zone is replaced by two spatially separated zones, with a fixed relative optical phase. When a molecule has passed through the first zone of interaction, it is in a coherent superposition of lower and upper levels. The coherence precesses freely between the two zones. In the second zone, the molecule is either excited or deexcited, depending on the relative phase between the excitation field and the coherence. Thus, fringes develop in the excitation probability versus the laser frequency, and their spacing depends on the transit time between the two zones.

In the optical domain, this method must be associated with a sub-Doppler technique in order to avoid scrambling of the fringe pattern. The use of saturated absorption and a three- or four-zone configuration [10,12,13,16] imposes severe conditions on parallelism and equidistances that, in practice, limit the distance between zones and, finally, the ultimate resolution. By contrast, in the case of two-photon spectroscopy only two zones are required, each comprising a standing wave, and the Doppler shift is compensated in each one [11,12,14,15]. The excitation probability for a molecule, of longitudinal velocity v_x, which crosses the centers of the two standing waves, is proportional to

$$\Omega_{\mathrm{eff}}^2\{1+\cos[2(\omega-\omega_{eg}/2)D/v_x+\Delta\Phi]\}\times\exp\left[-\left(\frac{\omega-\omega_{eg}/2}{v_x/w}\right)^2\right],$$

where $\Omega_{\mathrm{eff}}/2\pi$ is the effective Rabi frequency, D is the distance between zones, w is the laser beam radius, $\omega-\omega_{eg}/2$ is the laser frequency detuning from the two-photon resonance, and $\Delta\Phi$ is the relative phase of the standing wave between two zones. The experimental signal should exhibit fringes of spacing half the inverse of the transit time D/u between two zones for the mean velocity u. The contrast is unity if the

*Electronic address: amy@lpl.univ-paris13.fr
†Permanent address: The Cavendish Laboratory, Madingley Road, Cambridge CB3 OHE, UK.

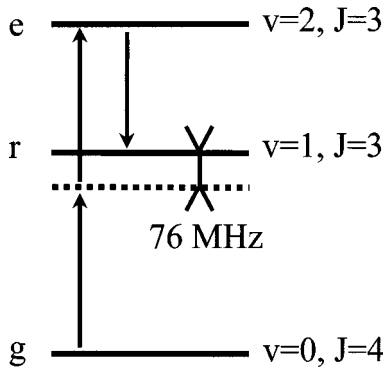

FIG. 1. Schematic of the three levels involved in the $P(4)$ E resonance.

observed transition is well isolated. The only constraint is that the relative phase $\Delta\Phi$ vanishes [12], which is easily fulfilled by generating both standing waves inside the same Fabry-Perot cavity. In addition, this guarantees that the central fringe coincides with the molecular resonance. The side fringes will be attenuated due to the longitudinal velocity dispersion and the entire pattern is superimposed on the broader two-photon signal arising from the absorption in one single zone.

This simple description of the Ramsey fringes was recently reviewed using a complete treatment of energy and momentum conservation [22]. The configuration with two spatially separated zones reveals a new subtlety. The fringes must then be interpreted as arising from the change of momentum of the molecules along the molecular beam. In this respect, it must be noticed that the area between the paths corresponding to the two excitation channels is negligible, which makes this interferometer insensitive to such external fields as rotation or gravity. This is a main advantage compared to the Ramsey-Bordé interferometer in the context of the frequency metrology.

III. EXPERIMENTAL APPARATUS

Preliminary 10-kHz two-photon Ramsey fringes were already observed on SF_6 elsewhere [19], with a resolution limited by the hyperfine structure and the laser linewidth. We plan to reach much higher resolution and have constructed an apparatus, with an adjustable interzone distance, to give fringes of periodicity 2 kHz to 100 Hz.

The SF_6 molecule, with high absorption characteristics and two-photon resonances, is well suited to high-resolution spectroscopy at 10.6 μm. Another good candidate would be OsO_4, because abundant isotopic species have no hyperfine structure, but no two-photon transition has yet been measured or calculated.

The experiment was performed on the $P(4)$ E transition of the $2\nu_3$ band of SF_6, which is at 174 MHz from the center of the $P(16)$ CO_2 laser line. Figure 1 gives the structure of the three levels involved, with a detuning from the intermediate level of 76 MHz. The two-photon transition was first measured by [20], who also pointed out its potential as a frequency standard.

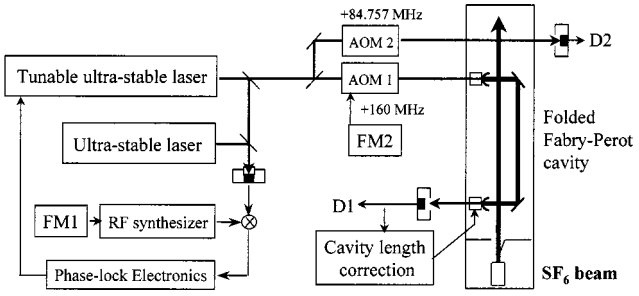

FIG. 2. Experimental scheme for two-photon Ramsey fringes. AOM denotes acousto-optic modulator; FM denotes frequency modulation.

The experimental setup is presented in Fig. 2. It is composed of three parts: the frequency-controlled laser system, the Fabry-Perot cavity, and the molecular-beam apparatus.

A. The laser sources

The performance of our frequency-controlled laser system has already been described in detail [3]. It employs two CO_2 lasers emitting in the 10-μm region. The first laser is frequency-locked to the $P(55)$ OsO_4 line located at 59 MHz from the center of the $P(16)$ CO_2 laser line [23]. The beat note between this laser and the second laser is then phase-locked to a tunable synthesizer. Thus, the stability acquired by the OsO_4 lock is transferred to the second laser, which is also tunable around the emission line of CO_2. The main stability characteristics are a laser linewidth of the order of 6 Hz [full width at half maximum (FWHM)] which is 2×10^{-13} in relative value, and an Allan variance of 0.1 Hz ($\Delta\upsilon/\upsilon=3.5\times10^{-15}$) for a time constant of 100 s. The reproducibility was estimated to be 10 Hz. This stability performance ensures that our experimental resolution will not be limited by the laser itself.

B. The folded Fabry-Perot cavity

A key point of the experiment is the generation of the two phase-coherent standing waves forming the two interaction zones for Ramsey spectroscopy. They are realized within a four-mirror folded Fabry-Perot cavity (FPC). The mirrors are mounted on an independent structure made from invar and graphite that is mechanically isolated from the vacuum chamber by graphite wool padding. The mirror mounts can be translated along the structure to adjust the interzone distance. The cavity is symmetric; the coupling mirrors are plano-concave with a 50-m curvature, while the folding mirrors are plane. The beam radius is almost constant inside the cavity; it is approximately 3 mm for a 10- or 20-cm interzone spacing. The laser feeds a cavity mode with a linear polarization, perpendicular to the plane of incidence. For that polarization, the reflectivity of each mirror is 99.8%, leading to a theoretical finesse of 500 (Appendix A). The corresponding measured value is 470.

Each concave mirror is mounted on a piezoelectric transducer (PZT) in order to modulate or adjust the cavity length, while the transmitted signal is used for locking the cavity resonance onto the laser frequency.

C. The molecular beam

The molecular-beam apparatus was designed for supersonic expansion of SF_6. This allows rotational cooling of the beam, and thus a strong enhancement in the population of the $J=4$ level. We use either a pure SF_6 or a He-seeded beam, with an input pressure of a few 10^5 Pa. The advantage of pure SF_6 is that the velocity is lower, so the transit time is longer and the resolution is better.

The apparatus is 3 m long with two vacuum chambers. The supersonic expansion arises from a 25- or 50-μm-diam nozzle in the first vacuum chamber, which is pumped by a diffusion pump and separated from the second chamber by a 500-μm-diam skimmer. The nozzle-skimmer distance may be adjusted in the range 5–15 mm. The experimental chamber is 2 m long and 250 mm in diameter, pumped upstream with an ionic pump and down stream with a cryogenic trap and a diffusion pump. All connections are designed to minimize the mechanical noise transmission from the primary pumps.

IV. BEAM CHARACTERIZATION

A. Mechanical methods

The beam profile was first characterized using a torsion pendulum[1] on the molecular stream. The rotation was measured optically and the partial flux deduced for different positions of the pendulum. This revealed a small horizontal deviation of a few mrad of the beam from the axis of the chamber, and that the divergence was given by the nozzle-skimmer distance and the skimmer aperture. The deviation increases linearly with the nozzle pressure at 20 cm downstream from the nozzle, indicating good functioning of the beam. This dependence ceased to be linear at 1.20 m downstream, when the residual pressure exceeded a few 10^{-4} Pa, showing the limit of free expansion due to the residual gas pressure.

Assuming a theoretical supersonic velocity of 350 m/s, we deduce a total flux of $\approx 10^{15}$ molecules per second for a 15-mm nozzle-skimmer distance and an input pressure of SF_6 of 5×10^5 Pa. This is consistent with a rate calculation or a simple measurement of increase of the pressure when there is no pumping in the second chamber.

The longitudinal velocity distribution was measured using the usual time-of-flight (TOF) technique. A mechanical chopper modulated the beam and the current of an open ionization gauge indicated the molecular flux. The experimental TOF curves were analyzed and compared with numerical simulations taking into account the chopper slit width and the classical velocity distribution $f(v)=A\,v^2\exp\{-[(v-u)/\Delta v]^2\}$, where u is the central velocity and Δv the longitudinal velocity dispersion. For a pure SF_6 beam obtained with an input pressure of 5×10^5 Pa, we measured a central velocity of 370 m/s and a longitudinal dispersion of 55 m/s. This is consistent with calculations [24], and with bibliographic data [25,26]. We also recorded TOF data for a He-seeded beam, with 2.5–25 % SF_6. The experimental value of the mean velocity coincided with that of an effective particle having the weighted mean molecular mass and heat capacity of the components of the expanded mixture, as it should in an ideal gas mixture [24]. This demonstrates the absence of clusters in the beam, which would have increased the effective weight and induced a slowing of the beam. The relative dispersion is 10–15 % less than with the pure beam, and this better translational cooling indicates that the other expansion parameters, such as the rotational cooling, would also be more favorable.

[1]This apparatus was loaned to us by Professor J. Baudon.

B. Optical methods

The first step of characterization of the beam gives no access to the partial flux in the $J=4$ level. This important information was obtained by performing linear absorption spectroscopy on the one-photon $P(4)\,E$ transition of the ν_3 band. Laser spectroscopy has already been widely used for state-selective diagnostics of a molecular beam [27]. Associated with the line shape and amplitude analysis, this optical method of detection completes the characterization of the beam.

1. Analysis of the linear absorption signal

The experimental setup is very simple: a laser beam crossed the molecular beam perpendicularly, and its absorption was monitored as a function of frequency. The laser frequency was shifted 240 MHz by acousto-optic modulators (AOM's) and tuned to the lower transition of Fig. 1. A slotted disk was used to chop the molecular beam, thus inducing a modulation of the absorption as detected through a lock-in amplifier. The laser parameters were chosen to maximize the population inversion, using rapid adiabatic passage (RAP) from the ground level to the excited level (see [28] and refs. therein).

The line shape is dominated by the Doppler broadening; the linewidth is typically $ku\Delta\theta$ for our experimental conditions, where $\Delta\theta$ is the beam divergence. But it is complicated by the fact that the modulation phase is not uniform as the beam diameter at the chopper is not negligible compared to the slot size. This induces an out-of-phase signal, with a dispersive line shape, and the in-phase line shape is deformed from a Gaussian absorption line shape in the wings.

The influence on the line shape of this phase dispersion and of the longitudinal velocity distribution was analyzed; see Appendix B. Figure 3 displays the in-phase and out-of-phase experimental signals, together with a simulation for the two spectra that reproduces the relative amplitudes very well. Note that the signal amplitudes are comparable for both phases, whereas no out-of-phase signal is expected when the beam diameter is small compared to the size of the chopper slot. Except in the wings, the in-phase line shape is correctly fitted with a Gaussian, the center and width of which give, with good precision, the deviation and divergence of the beam. In this case, the effect of the dispersion of the phase of the modulation can be neglected.

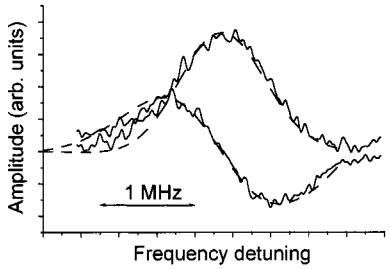

FIG. 3. Linear absorption of the $P(4)$ E resonance of the ν_3 band of SF_6. Continuous lines correspond to the two experimental absorption spectra, in phase with the modulation (Gaussian shape) and out of phase. They were recorded at 20 cm from the nozzle, with the same vertical scale, and with the following experimental conditions: 5×10^5 Pa pure SF_6 beam, nozzle-skimmer distance 15 mm, 40-μW power. Dashed lines correspond to a numerical simulation for the two phases with a divergence parameter $\Delta\theta = 32$ mrad and $\alpha = 85$ mrad (see Appendix B).

2. Divergence, deviation, fractional condensation, and temperature of the beam

The absorption was first recorded at 20 cm from the nozzle, giving typical linewidths of 1–2 MHz. The resulting deviation and divergence were consistent with the ones obtained with the torsion pendulum. The total divergence depends, however, on the input pressure; it increases by approximately 30% when the pressure is raised from 1×10^5 to 5×10^5 Pa.

We also checked that the signal amplitude increased linearly with the input pressure. This indicates the absence of clusters in the beam, at least up to 5×10^5 Pa.

Finally, we tried to record the absorption on other lines but with a high J value, for instance $Q(40)\,A_1^0$ or $Q(40)\,F_1^1$ [29]. The lack of signal, although the apparatus had the sensitivity to record some absorption with an amplitude reduced by more than 10, indicates that the temperature of our beam is below 30 K.

3. Estimation of the flux

The signal amplitude was then analyzed to obtain the partial flux in the $J=4$ level. This depends on the absorption probability and the laser divergence, and the geometrical factor for the overlap of laser and molecular beams. The maximum absorption signal is reached in the RAP regime, which leads to a total population inversion.

In the interaction, an expanded laser beam (radius $\approx$5.5 mm) crosses the major part of the molecular beam. It was slowly convergent ($\theta_L \approx 2$ mrad) with a power corresponding to a few π pulses.[2] Figure 4 displays the square root of the absorption signal against the square root of the laser power, in reduced units. The experimental signal first increased linearly, then saturated, indicating the beginning of the RAP regime. At this power level, a few tens of μW,

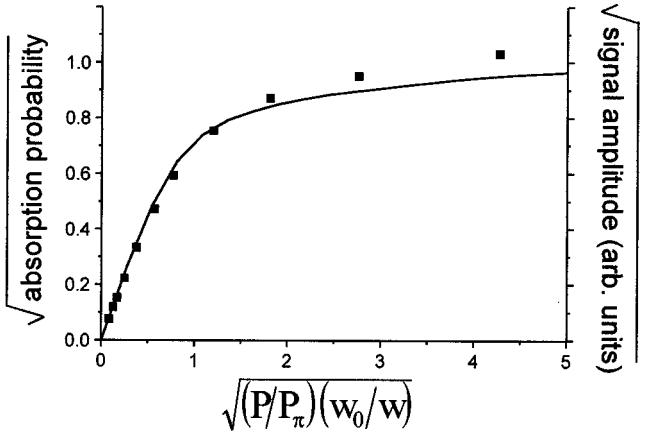

FIG. 4. Square root of the linear absorption signal, against the square root of the laser power, in the reduced unit of $\sqrt{(P/P_x)(w_0/w)}$. Square points correspond to experimental data on the $P(4)$ E resonance of the ν_3 band of SF_6 with the experimental conditions: pure SF_6 beam at 5×10^5 Pa with a velocity of 370 m/s, nozzle-skimmer distance 15 mm, beam diameter 10 mm, laser divergence 2 mrad, and diameter 11 mm. The continuous line corresponds to a simulation of the average absorption probability for the different molecular trajectories in a plane perpendicular to the laser beam. The experimental data were multiplied by an arbitrary factor to adjust them to the vertical scale of the simulation.

noise is proportional to laser power. Thus, to optimize the signal-to-noise ratio we limited the power to a level just approaching the regime of RAP. We are in neither the weak-field regime nor the strong-field regime (saturation parameter $\gg$1) with these conditions. This situation is described and simulated in [30] for the case of molecules crossing the center of the laser beam. The experimental case here is somewhat different since most of the molecules do not cross the center and thus experience a reduced power.

Saturation is best parametrized in $\sqrt{(P/P_\pi)(w_0/w)}$ as in Fig. 4 since, in the divergent part of the beam, the useful power is the power reduced by the ratio of the laser beam radius to the waist. Thus for our laser characteristics, onset of saturation corresponds to five π pulses, that is, 1 on the x axis. The continuous line of Fig. 4 corresponds to a simulation of the averaged transition probability for the different molecular trajectories in a plane perpendicular to the laser beam [31]. It clearly fits very well with the experimental points for power not exceeding two reduced units, particularly since there is no adjustment of the horizontal scale. This also demonstrates that the mean transition probability for molecules having zero velocity along the laser beam is approximately 0.6 at onset of saturation, and increases slowly. Note that we also took into account the velocity distribution, which changes the interaction time and thus the pulse area, but it does not influence the probability by more than a few percent.

The molecular-beam spread along the laser beam must also be taken into account which will increase the averaged transition probability at higher powers. This is the origin of the deviation of the experimental points from the simulation on Fig. 4. Since the transit width is small compared to the

[2]The π-pulse power is 18 μW for that transition and a mean velocity of 370 m/s [29].

residual Doppler width, the averaged absorption probability for the whole beam is at least $0.6(\theta_L/\Delta\theta)$ at onset of saturation. The factor in parentheses is approximately 0.06 in our experimental conditions.

As a result, we measured, at a distance of 20 cm from the nozzle, a partial flux of $\approx 5\times 10^{12}$ molecules per second in the $J=4$ level for an input pressure of 5×10^5 Pa and a 15-mm nozzle-skimmer distance. Assuming a temperature of 30 K, this corresponds to a total flux of approximately 10^{15} molecules per second, which is consistent with our previous measurement.

We also recorded the absorption at different distances, 70 and 120 cm, from the nozzle. For 70 cm, the reduction of flux is well described by the beam divergence, taking into account the different geometrical overlap and transition probability compared to the experiment at 20 cm. But these parameters can explain only half the reduction of flux at 120 cm, which indicates that the molecular beam begins to be destroyed by the residual gas, of which the pressure is a few 10^{-4} Pa.

V. HIGH-RESOLUTION SPECTROSCOPY

A. Detection methods

Two different optical detection methods may be used. The first possibility is to record the transmission signal of the cavity, detection channel $D1$ in Fig. 2, taking advantage of the enhancement of the signal contrast due to the cavity (Appendix A). The laser frequency is modulated through the synthesizer, which drives the phase-lock loop. Alternatively, the signal can be read downstream of the interaction by probing the molecular-beam absorption on the upper one-photon transition with an auxiliary beam, detection channel $D2$ in Fig. 2. This is very similar to the RAP experiment described in Sec. IV. To record the fringes, the modulation depth was small enough that modulation could be applied to the radio-frequency driving the AOM 1. In this method, the auxiliary beam was not modulated. The signal arose from a modulation transfer from the molecular beam to the laser beam and there was, thus, no background.

B. Saturated absorption

As an intermediate step towards Ramsey fringes, a saturated absorption signal within the Fabry-Perot cavity was first detected in order to test and optimize the cavity performance and the detection methods.

The laser frequency was shifted by both AOM's of Fig. 2 and tuned to the lower one-photon resonance. The laser beam fed the FPC, of which the interzone separation was 50 cm. Figure 5 displays a typical spectrum for an input pressure of 5×10^5 Pa. The signal was detected on the beam transmitted by the FPC after demodulation at 20 kHz, which corresponds to the laser frequency modulation. It fits very well with the derivative of a Gaussian. This line shape has a 40-kHz peak-to-peak width that corresponds to the convolution of the hyperfine structure and the individual components broadened by the transit effect through just one zone. Note that the SNR is quite low although the detection process

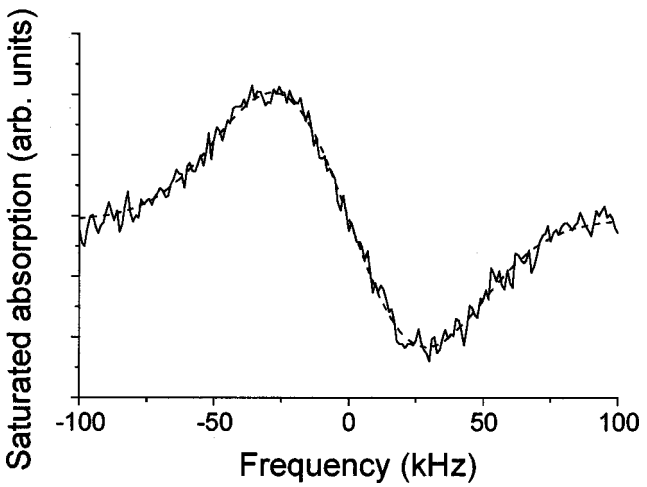

FIG. 5. Saturated absorption signal detected on the cavity transmission beam using a laser FM of 20 kHz. Typical conditions: 10 μW in the cavity, 5×10^5 Pa pure SF_6 beam. Data are fitted with the derivative of a Gaussian.

allows a gain of 300 on the contrast. The transmitted beam was indeed noisy, and this prevented the observation of two-photon absorption with this configuration.

The noise results mainly from the instability of the FPC. The cavity noise exhibits low-frequency peaks, which prevent any increase in the gain and the bandwidth of the servo loop of the cavity length. These peaks were reduced after better isolation between cavity and chamber and when the cavity rigidity was improved. Figure 5 was recorded after part of this improvement. Then an 8-cm spacing between zones was employed to improve further the FPC stability. The noise reduced simultaneously and this allowed us to detect Ramsey fringes in the best conditions (see Sec. V C).

Another important source of power instability originates in back reflections of the laser beam from the cavity. The coupling between laser and cavity mode is made with a telescope, and was optimized with filtering of the laser mode. The reflected beam intensity was also minimized, by using antireflection optics composed of a polarizer plus a quarter-wave plate and attenuators.

Finally, we observed the laser frequency stability by recording the beat note with a third laser in another room. We could check that the vibration of the pumping system did not degrade the stability of the spectrometer.

C. Two-photon Ramsey fringes with an 8-cm interzone spacing

Figure 6 displays an ultrahigh resolution two-photon spectrum for an 8-cm spacing between zones [32]. The central part exhibits Ramsey fringes with more than 10 oscillations, which are superimposed on the broader signal arising from the two-photon absorption in a single zone. The fringes were recorded on the transmission signal of the cavity for an input pressure of 5×10^5 Pa pure SF_6 and a 5-mm nozzle-skimmer distance. The laser frequency was modulated at 1.012 kHz with a depth of 500 Hz. Optimal power in the

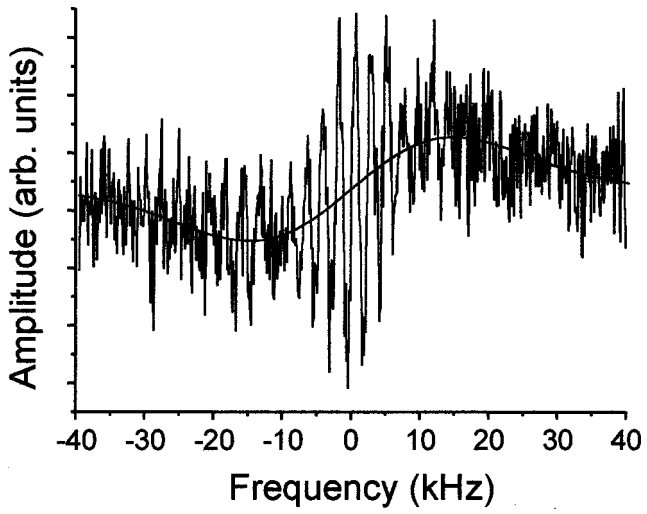

FIG. 6. Two-photon absorption signal detected on the cavity transmission beam. Experimental conditions: laser FM at 1.012 kHz, depth 500 Hz, 16 mW in the cavity, 5×10^5 Pa pure SF_6 beam, accumulation time 2.4 s/point. Data are fitted with the derivative of a Gaussian.

folded standing wave was about 16 mW, which corresponds roughly to a $\pi/2$ pulse for the two-photon transition. The accumulation time per point is 2.4 s. The background signal fits very well with the derivative of a Gaussian, of peak-to-peak width 30 kHz. The line shape is a convolution of the transit line shape, peak-to-peak width 28 kHz, with the hyperfine structure.[3] The central part of the spectrum, corresponding to the main hyperfine component, has been fitted with a sine superimposed on a slope, resulting in a fringe periodicity of 2.3 kHz and a relative determination of the central frequency with precision better than 10 Hz. This is limited by the signal-to-noise ratio (SNR), which is approximately 3 for 1 s of averaging. As a comparison, the four-zone saturated absorption developed earlier led to 10.42-kHz fringes with a SNR of 6 for 1 s of averaging [16]. The periodicity is consistent with the theoretical value $u/2D$ (see Sec. II) with $u=370$ m/s and $D=8$ cm. The absolute frequency 28 412 764 347.0 (2) kHz was determined using the OsO_4 frequency grid [23] as recently updated [34] and agrees with the previous measurement [7]. The contributions of other hyperfine components are less visible but their positions are consistent with the values given above.

Fringes were recorded in similar conditions for an input pressure of 3×10^5 Pa. The amplitude was reduced proportionally, which indicates good functioning of the molecular beam up to a pressure of 5×10^5 Pa.

We also varied the distance between nozzle and skimmer between 5 and 15 mm, checking that the fringe amplitudes were decreasing linearly with this distance. The molecular-beam diameter in the second zone is indeed larger than the laser diameter. Thus the change of the molecular-beam size perpendicular to the laser beam does not influence the number of molecules interacting with the laser. The gain concerns only the direction along the laser beam.

The modulation parameters were adjusted to optimize the SNR. With half the modulation frequency and the same modulation index, the signal was 30% higher, but the noise increased approximately two times. Since frequency and depth are not negligible compared to the fringe periodicity, the line shape would differ slightly from the simple derivative of the two-photon signal, and this could induce a small reduction of the contrast.

With this FM detection, the amplitude of the fringes should be greatly enhanced compared to the two-photon absorption background, but this is obviously not the case. In fact, the spectrum corresponds to a contrast of only 1/25. This results partly from the molecular-beam divergence since there are 35% fewer molecules crossing the second zone of interaction, which multiplies the contrast by 0.8, and partly from the hyperfine structure because of the superposition of the background signals for the different hyperfine components, which leads to another factor of approximately 0.6. This implies that the fringes arise from roughly one order of magnitude fewer molecules than expected. For the central component, only a few 10^{10} molecules per second contribute to the interference signal. This loss of signal can be partly attributed to the imperfect alignment of the two zones relative to the beam axis. It could also be due to a partial molecular decoherence between the zones caused by small-angle collisions in the beam that dephase the molecular coherence, or to the Zeeman effect. Either will give a partial scrambling of the fringe pattern.

Fringes were also recorded by detection channel $D2$ (see Fig. 2) using rapid adiabatic passage. They exhibited a little smaller SNR (2 for 1 s) while the signal itself was reduced by roughly an order of magnitude. Due to this loss of signal, which probably has the same origin as the loss of contrast, we were not able to compare the two detection channels. This detection channel, however, which has theoretically no background, should benefit from an active reduction of the laser intensity noise.

D. Increase of the resolution with a 20-cm interzone spacing

As a second step, to increase the resolution, some fringes were recorded with a 20-cm interzone spacing. With a pure SF_6 beam, the SNR was degraded to about 1 for 10-s averaging time.

To overcome this problem, we decided to seed the beam with He, since its supersonic expansion has better performance. Also channeling of the heavier SF_6 molecules inside the He beam enhances the partial flux in the beam center. Figure 7 presents a typical spectrum obtained with 25% SF_6 in He and a 20-cm interzone spacing. Data are fitted with a sine superimposed on a slope, giving a periodicity of 1.5 kHz. This is consistent with the faster speed of 590 m/s of the molecules. The fringes were recorded on the transmission of the cavity for a total input pressure of 5×10^5 Pa. The laser frequency was modulated at 462 Hz with a depth of 400

[3]The two-photon resonance is composed of four main hyperfine components spanning 40 kHz with the following relative amplitudes and positions: 0.68 at -11.78 kHz, 1 at 0 kHz, 0.46 at $+7.43$ kHz, and 0.24 at $+17.06$ kHz [7,33].

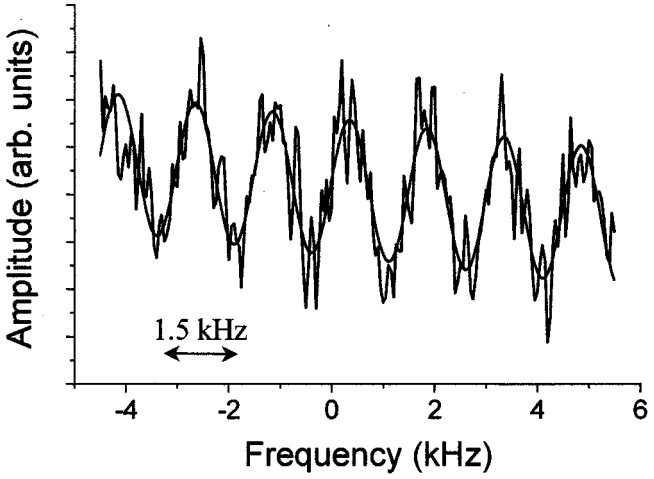

FIG. 7. Fringes detected on the cavity transmission beam. Experimental conditions: FM applied on the laser PZT at 462 Hz, depth 400 Hz, 26 mW in the cavity, 25% SF_6 beam at 5×10^5 Pa, accumulation time 5 s/point. Data are fitted with a sine superimposed on a slope.

Hz. Due to the limited power available from the laser, the power in the standing wave was only 26 mW. This is now not sufficient to apply a $\pi/2$ pulse, since the molecular velocity is increased. The SNR is roughly 2 for a 1-s averaging time.

On reducing the proportion of SF_6, the resolution decreased but the signal increased, which illustrates the better rotational cooling. Figure 8 displays a spectrum with 7.5% SF_6. The periodicity is 2.3 kHz as with a pure SF_6 beam and an 8-cm interzone spacing, but the SNR is now 10 for 1 s, and we were able to define the line center within 6 Hz.

VI. CONCLUSION

In this paper, we present our results of ultrahigh-resolution spectroscopy in the 10-μm region using a molecular beam of SF_6. The beam was characterized by analyzing the linear absorption line shape and amplitude. We demonstrated two-photon Ramsey fringes on a 1.5-kHz periodicity, which improves by a factor of 7 the periodicity obtained on a saturated absorption resonance of SF_6 [16]. The fringes were obtained using a 20-cm interzone separation, which demonstrates the experimental advantage of a two-photon configuration. The achieved resolution compares very well with that obtained in the optical domain using Ramsey spectroscopy as, for example, the 1-kHz periodicity using Ca at 657 nm in a magneto-optical trap with time-separated fields [35] or the 5-kHz periodicity of the two-photon $1S$-$2S$ transition at 243 nm in hydrogen [36].

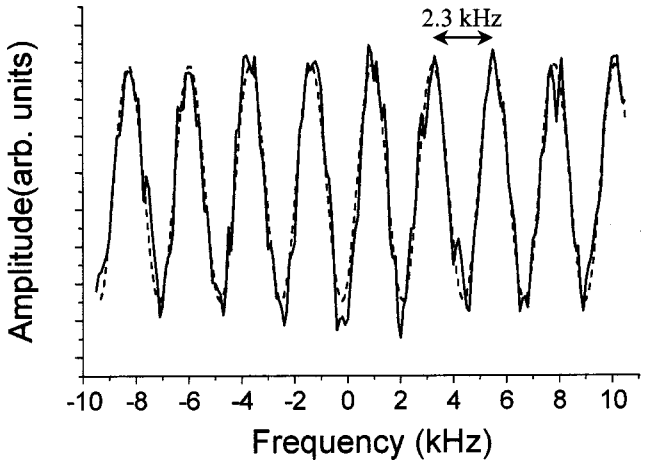

FIG. 8. Fringes detected on the cavity transmission beam. Experimental conditions: FM applied on the laser PZT at 962 Hz, depth 400 Hz, 14 mW in the cavity, 7.5% SF_6 beam at 5.5×10^5 Pa, accumulation time 1.6 s/point. Data are fitted with a sine superimposed on a slope.

The present results represent a first step in this experiment, since we demonstrated that only a fraction of molecules of the beam contributes to the fringes signal. The fringe linewidth of 375 or 575 Hz [half-width at half maximum (HWHM)] is comparable to the 280-Hz linewidth (HWHM) achieved with the detection of slow molecules in a cell [7], using the same transition. But the present SNR of 10 for a 1-s integration time is seven times better.

We plan to modify the expansion system to improve the beam performance. The resolution might then be improved by an order of magnitude. Although the contrast of the fringes is less than expected, the signal is in fact very strong (a few 10^{10} mol/s, i.e., 1 nW). Thus, the SNR is mainly limited by the strong technical noise that is inherent in any absorption detection method. This suggests that we might improve the SNR dramatically by a better detection technique, such as using state-selective ionization. Thus, the Ramsey setup seems very promising because there is considerable room for both signal improvement and noise reduction. Concerning the metrological features, the systematic effects are either very small or can be easily and precisely measured or calculated, with the possible exception of the black body radiation shift [37]. This system is thus a very serious candidate for a frequency standard in the infrared region with a potential accuracy in the 10^{-15} range.

ACKNOWLEDGMENTS

We appreciated fruitful discussions with Ch. J. Bordé and useful advice from G. Scoles and J. Baudon on the optimization of the molecular beam. This work has been supported by the Bureau National de Métrologie, the ETCA-DRET, the European Union through two HCM programs, and Gonville and Caius College, Cambridge.

APPENDIX A

This appendix gives the different characteristics of the folded Fabry-Perot cavity. For T_1 and T_2, the intensity transmission coefficient of the coupling and folding mirrors, respectively, the finesse is given by $F=\pi/(T_1+2T_2)$. At resonance, for an incident intensity I_i, the intensity inside the cavity is $I_C/I_i=T_1/(T_1+2T_2)^2$, the reflected intensity is $I_R/I_i=[2T_2/(T_1+2T_2)]^2$, and the transmitted intensity is $I_T/I_i=T_1^2/(T_1+2T_2)^2$. The signal contrast on the transmitted beam is enhanced by a factor $2F/\pi$.

The mirror specifications give $I_C/I_i=55$, $I_R/I_i=0.44$, $I_T/I_i=0.11$, and a finesse of 500 for *S* polarization, while the measured value is 470. The gain in contrast is then of the order of 300. The experimental finesse is ≈170 for the *P* polarization, and the cavity resonances are also different.

APPENDIX B

This appendix details the analysis of the linear absorption line shape in the molecular beam.

The function $a(v,\theta,\omega)$ represents the absorption for an elementary part of the beam of longitudinal velocity v and inclination θ to the beam axis. $a(v,\theta,\omega)=f(v)g(\theta)\exp(-[(\omega-kv\theta)/\gamma]^2)$, where $f(v)=Av^2\exp(-[(v-u)/\Delta v]^2)$ is the usual velocity distribution for a supersonic beam, we assume a Gaussian divergence shape $g(\theta)=\exp(-[(\theta-\theta_0)/\Delta\theta]^2)$, and γ is the transition width. The total absorption signal results from the double integration of $a(v,\theta,\omega)$ over velocity and angle, weighted by the phase-dispersion factor $\cos(\varphi(v,\theta))$. This factor $\cos[\varphi-\pi\theta/\alpha-2\pi d/(vT)]$ contains two terms in addition to the lock-in amplifier phase φ: the first one depends on the angle of view α of a disk slot from the beam origin, and the second one depends on the ratio of the transit time d/v between chopper and laser beam to the slot rotation period T.

All the parameters u, Δv, α, φ, d, and T are well known, except γ. This last is of the order of the transit width: $\gamma/2\pi\approx 50$ kHz, which has no influence on the line shape as this is mainly governed by the Doppler broadening $ku\Delta\theta/2\pi\approx 1$ or 2 MHz. We chose the chopper period so that the factor $d/(vT)$ was approximately constant over the velocity distribution so that the integral over the longitudinal velocities would not influence the line shape. For example, the factor changes only ± 15% for $1/T\approx 750$ Hz and $d=15$ cm.

By contrast, the line shape is governed by the beam divergence $\Delta\theta$ and deviation θ_0. The line is centered at $ku\Delta\theta$, and evolves from a quasi-Gaussian line shape (''in-phase''), the linewidth of which is proportional to $\Delta\theta$, to a dispersive line shape (''out-of-phase''). The ratio of the in-phase and out-of-phase amplitudes is $2.4\ \alpha/\Delta\theta$.

[1] C. Freed and A. Javan, Appl. Phys. Lett. **17**, 53 (1970).
[2] O. Acef, IEEE Trans. Instrum. Meas. **46**, 162 (1997).
[3] V. Bernard *et al.*, IEEE J. Quantum Electron. **QE-33**, 1282 (1997).
[4] Ch. Daussy, F. Ducos, G. D. Rovera, and O. Acef, IEEE Trans. Ultrason. Ferroelectr. Freq. Control **47**, 518 (2000).
[5] S. N. Bagayev, A. E. Baklanov, V. P. Chebotayev, and A. S. Dychkov, Rev. Roum. Phys. **33**, 361 (1988).
[6] Ch. Chardonnet, F. Guernet, G. Charton, and Ch. J. Bordé, Appl. Phys. B: Lasers Opt. **59**, 333 (1994).
[7] P. E. Durand *et al.*, Europhys. Lett. **37**, 103 (1997).
[8] A. Fioretti *et al.*, Phys. Rev. Lett. **80**, 4402 (1999).
[9] N. F. Ramsey, Phys. Rev. **78**, 695 (1950).
[10] Y. V. Baklanov, B. Y. Dubetsky, and V. P. Chebotayev, Appl. Phys. **9**, 171 (1976).
[11] Y. V. Baklanov, V. P. Chebotayev, and B. Y. Dubetsky, Appl. Phys. **11**, 201 (1976).
[12] Ch. J. Bordé, C. R. Séances Acad. Sci., Ser. B **284**, 101 (1977).
[13] J. C. Bergquist, S. A. Lee, and J. L. Hall, Phys. Rev. Lett. **38**, 159 (1977).
[14] M. M. Salour and C. Cohen-Tannoudji, Phys. Rev. Lett. **38**, 757 (1977).
[15] V. P. Chebotayev, A. V. Shishayev, B. Ya. Yurshin, and L. S. Vasilenko, Appl. Phys. **15**, 43 (1978).
[16] Ch. J. Bordé *et al.*, Phys. Rev. A **30**, 1836 (1984).
[17] A. G. Adam *et al.*, Phys. Rev. A **34**, 4803 (1986).
[18] M. P. Sassi, M. Q. Pisani, M. Zucco, and C. Foglia, in *Proceedings of the 5th Symposium on Frequency Standards and Metrology* (World Scientific, Singapore, 1996).
[19] A. Linskens, Ph.D. thesis, University of Nijmegen, 1994.
[20] A. Linskens, S. te Lintel Hekkert, and J. Reuss, Infrared Phys. **32**, 259 (1991).
[21] F. Herlemont, M. Khelkhal, J. Legrand, and G. Pierre, Opt. Lett. **23**, 957 (1998).
[22] Ch. J. Bordé, in *Atom Interferometry*, edited by P. R. Berman (Academic, San Diego, 1977), pp. 257–292.
[23] Ch. Chardonnet and Ch. J. Bordé, J. Mol. Spectrosc. **167**, 71 (1994).
[24] D. R. Miller, in *Atomic and Molecular Beam Methods*, edited by G. Scoles (Oxford University Press, New York, 1988), pp. 14–53.
[25] D. Bassi, A. Boschetti, M. Scotoni, and M. Zen, Appl. Phys. B: Photophys. Laser Chem. **26**, 99 (1981).
[26] S. Mohr, graduate thesis, Max-Planck-Institut für Strömungsforschung, Göttingen, Germany, 1990 (unpublished).
[27] U. Hefter and K. Bergmann, in *Atomic and Molecular Beam Methods*, edited by G. Scoles (Oxford University Press, New York, 1988), pp. 193–253.
[28] C. Liedenbaum, S. Stolte, and J. Reuss, Phys. Rep. **178**, 1 (1989).
[29] Ch. J. Bordé, Rev. Cethedec-Ondes et Signal **NS 83-1**, 1 (1982).
[30] Ch. J. Bordé, Ch. Chardonnet, and D. Mayou, in *Laser Spectroscopy VIII*, edited by S. Svanberg (Springer-Verlag, Berlin, 1987), pp. 381–385.
[31] L. F. Constantin, Ph.D. thesis, Université Paris 13, France, 2000 (unpublished).
[32] L. F. Constantin *et al.*, Phys. Rev. A **60**, R753 (1999).
[33] P. E. Durand, Ph.D. thesis, Université Paris 13, France, 1997 (unpublished).
[34] O. Acef, F. Michaud, and G. V. Rovera, IEEE Trans. Instrum. Meas. **48**, 567 (1999).
[35] F. Riehle *et al.*, Laser Phys. **8**, 664 (1998).
[36] A. Huber, B. Gross, M. Weitz, and T. W. Hänsch, Phys. Rev. A **58**, R2631 (1998).
[37] A. Amy-Klein *et al.*, Opt. Express **4**, 67 (1999).